Active Nordic Seas deep-water formation during the last glacial maximum

Christina S. Larkin[1,2,3*], Mohamed M. Ezat[1,4,5], Natalie L. Roberts[1], Henning A. Bauch[6,7], Robert F. Spielhagen[7], Riko Noormets[8], Leonid Polyak[9], Steven G. Moreton[10], Tine L. Rasmussen[4], Michael Sarnthein[11], Edward T. Tipper[1], Alex M. Piotrowski[1,3]

Affiliations:

[1]Department of Earth Sciences, University of Cambridge, Downing Street, UK. [2]School of Ocean and Earth Science, University of Southampton, National Oceanography Centre, UK. [3]Murray Edwards College, University of Cambridge, Huntingdon Road, Cambridge, UK. [4]CAGE – Centre for Arctic Gas Hydrate, Environment and Climate, Department of Geosciences, UiT the Arctic University of Norway, Tromsø, Norway.[5]Department of Geology, Faculty of Science, Beni-Suef University, Beni-Suef, Egypt. [6]Alfred Wegener Institute for Polar and Marine Research, Bremerhaven, Germany. [7]GEOMAR Helmholtz Centre for Ocean Research, Kiel, Germany. [8]The University Centre in Svalbard, Norway.[9]Byrd Polar and Climate Research Center, Ohio State University, USA [10]NERC Radiocarbon Facility, East Kilbride, UK. [11]Christian-Albrechts University, Kiel, Germany. *e-mail: c.s.larkin@soton.ac.uk

The Nordic Seas are the primary location where the warm waters of the North Atlantic Current densify to form North Atlantic Deep Water, which plays a key part in the modern Atlantic Meridional Overturning Circulation. The formation

of dense water in the Nordic Seas and Arctic Ocean and resulting ocean circulation changes were likely driven by and contributed to the regional and global climate of the last glacial maximum (LGM). Here, we map the source and degree of mixing of deep-water in the Nordic Seas, and through the Arctic Gateway (Yermak Plateau) over the last 35 thousand years using neodymium isotopes (εNd) measured on authigenic phases in deep-sea sediments with a high spatial and temporal resolution. We find that a large-scale reorganisation of deep-water formation in the Nordic Seas took place between the LGM (23-18 thousand years ago) and the rapid climate shift that accompanied the subsequent deglaciation (18-10 thousand years ago). We show that homogeneous εNd signatures across a wide range of sites support LGM deep-water formation in the Nordic Seas. In contrast, during the deglaciation disparate and spatially variable εNd values are observed leading to the conclusion that deep-water formation may have been reduced during this time.

Deep-water formation processes in the Nordic Seas regulate the global climate via the redistribution of heat by the surface ocean and the capacity of the deep ocean to store carbon[1]. At present the Atlantic Meridional Overturning Circulation (AMOC) links polar and sub-polar climate with the formation of North Atlantic Deep Water (NADW), a major component of the global oceanic thermohaline circulation. The densest northern-sourced waters in the modern AMOC are formed in the Nordic Seas, primarily by deep convection and gradual transformation of North Atlantic surface waters[2].

These dense waters formed in the modern Nordic Seas overflow the Greenland-Scotland Ridge (GSR), eventually contributing to NADW accumulating carbon and nutrients as it flows throughout the deep ocean[2] (Fig. 1). The extent, mechanism, and importance of deep-water formation in the Nordic Seas during glacial periods and periods of ice rafting during meltwater events (Heinrich Events/Heinrich Stadials) are still not adequately understood. The canonical view is that the glacial AMOC was displaced from the Nordic Seas to south of Iceland in the form of a fast and shallow overturning cell forming Glacial North Atlantic Intermediate Water and that there was Southern-sourced water in the deep (> 2.5 km) Atlantic[e.g,3]. Contrary to this several studies[e.g.4,5] argue for the presence of glacial NADW and speculate that this dense water may have been sourced from the Nordic Seas. Keigwin and Swift[6] similarly suggest that a Northern-sourced water mass may have been present in the deep (~ 5000 m) Atlantic, which could plausibly have been sourced from the Nordic Seas[7]. However, proposed scenarios of LGM deep-water formation in the Nordic Seas range from near-cessation to vigorous present-day-like deep-water formation[8–11].

There is evidence supporting a continued or intermittent subsurface inflow of the North Atlantic Current (NAC) during the LGM[12,13] to the Norwegian Sea. Polynya formation proximal to ice-sheets has been inferred, ventilating parts of the LGM deep Nordic Seas[7,9,14]. Several proxy studies indicate a persistent overflow from the Nordic Seas into the glacial Atlantic Ocean[8,15,16]. However, warmer waters (~ 1 to 2^{o}C warmer than the modern) in the intermediate to deep Nordic Seas and Arctic[11,17,18] indicate a reduced heat release to the atmosphere and less net cooling of the NAC waters, which could be due to subsurface expansion and deepening of the NAC[13,19]. This does not support widespread deep-water formation by brine

rejection or modern-like open-ocean convection, which would produce cooler waters at depth. Nevertheless, periodic cooler bottom water temperatures have been observed in LGM-aged sediments near Svalbard and in the Lofoten Basin[18,20]. Less efficient deep-water formation via convective processes, upwelling, slow modification and return of Atlantic waters, or small-scale brine formation at shelf edges could be consistent with studies to date.

Ultimately, the question of Nordic Seas deep-water formation during the LGM and its geographical extent remains an open debate which has not yet been fully constrained by proxy studies. Resolving the location and extent of deep-water formation under glacial conditions is key to understanding the link between climate, the oceans, ice-sheets, heat transport and carbon cycling. In this study, therefore, we provide, at a high spatial and temporal resolution, a depiction of past Nordic Seas circulation under glacial conditions.

Neodymium isotope tracing of ocean circulation

Neodymium (Nd) isotopes measured on authigenic phases (authigenic εNd) are a powerful tool used to trace water mass circulation[21]. εNd is a proxy of the source of the Nd in the water mass. Spatial records can be related to each other to trace the flow path of water masses, and deduce their mixing with other water masses, so long as new sources of Nd are not added. However, the local input of Nd to water masses[22,23] can also alter the dissolved seawater εNd composition. This is likely to be of greater relative importance in controlling spatial patterns of εNd during times of reduced advection.

We measured εNd on mixed planktic foraminifera, which were not reductively cleaned of authigenic coatings and thus represent bottom water[24], and weak acid-reductive sediment leaches from a wide range of deep-sea sediment core sites in the Arctic Ocean and Nordic Seas. This is combined with published records to produce a high spatial and temporal resolution (Fig. 1) allowing us to place the magnitude of proxy shifts into a regional context and distinguish large scale changes linked to hydrographic transport and mixing from small-scale variability due to local inputs. Detailed information on samples and analytical methods is given in the Methods and Extended Data Figures 1,2,3 and 4.

Previous proxy studies in this region have often focused on only a handful of core sites. Traditional proxy studies (e.g. $\delta^{13}C$) based on epifaunal benthic foraminifera are hampered by the scarcity of suitable foraminifera in this region and, therefore, lack a holistic approach. Moreover, studies based on palaeotemperature reconstructions and radiocarbon ventilation ages fail to provide information on larger-scale, long-term, water-mass homogenisation and extent and, therefore, direct evidence for prolonged deep-water formation and its geographical range. Sea surface temperature and biomarker studies and studies based on foraminiferal calcite have the potential to be biased by highly variable year-on-year and seasonal conditions[25], potentially masking a true, time-integrated climate and oceanographic signature. Our approach, in contrast, provides a different insight because it integrates seasonal and multi-annual variability. εNd integrates longer-term ocean processes due to the relatively long residence time of Nd in the ocean (~ 200-1000 years) and the way the signature is continually incorporated into sediments in early authigenic phases, making it sensitive to hydrographic changes which occur on this timescale.

High resolution εNd

We measured authigenic εNd in 17 core sites to map out the geographical extent and consistency, or inconsistency, of Nordic Sea water-mass compositions from the last glacial period (~ 35 ka) to the late Holocene (< 5 ka). Individual core records from selected high-resolution core sites are shown in Fig. 2. Data are compared to similar records from the NE Atlantic and central Arctic Ocean as records in Fig. 2 and are also presented as time-slice cross sections in Fig. 3. Due to the high resolution of this data set and to understand the larger scale pattern of εNd, the data are temporally averaged. The data group naturally into 3 equal sized (5 ka) time intervals (Fig. 4), comprising the late Holocene (5-0 ka), the deglaciation (18-13 ka) and the LGM (23-18 ka). This compilation is focused on the Nordic Seas and Arctic Gateway (Yermak Plateau). The data are shown as probability density plots and histograms (Fig. 4). We compare the late Holocene with seawater values from the same depth and latitudinal range (Fig. 4), as well as to the LGM and deglacial values. These datasets were also compared using statistical tests (details are given in the Methods and Extended Data Fig. 5 and Extended Data Tables 1 and 2).

The late Holocene compositions (0-5 ka) observed in the Nordic Seas and Yermak Plateau show the same spatial patterns (Fig 3A,B) and variability (Fig 4) as the modern across a range of core sites from the shallowest (at 488 m water depth, today bathed in warm northward flowing Atlantic waters on the Yermak Plateau) to the deepest in the Greenland Sea (3050 m water depth). This demonstrates that for the late Holocene, a seawater-derived signature is recorded with εNd on authigenic

phases. In addition, the similar spatial pattern to the modern implies a hydrographic link between the inflow and deeper regions in the Nordic Seas and the Yermak Plateau. The homogeneity of the modern and late Holocene dataset relative to the large Nd isotope range of potential sources (which span almost the entire crustal array of εNd, ~ -40 on Greenland, to ~ 10 on Iceland) also indicates vigorous circulation acting to homogenize compositions in the Nordic Sea, with a value of ~-10 (Fig. 4).

The Yermak Plateau provides the ideal locality to test for changes in the NAC composition over time, because this is where warm high salinity Atlantic-derived sub-surface waters are in contact with the sediment-water interface[26,27]. A shallow sediment core from the Yermak Plateau (Fig. 2c, at 488 m) is used to monitor past changes in this Atlantic-derived endmember. Many studies indicate the continued strong influence of warm Atlantic waters in this region at the LGM, including at this core site[12,26]. We compare this shallow core site to two other cores at different water depths (798 m and 2531 m). These Yermak Plateau cores sites have differing sedimentation rates (4, 6 and 10 cm/kyr) and likely distinctive sediment provenances[28]. All the sites show similar changes through time (Fig. 2c). The three core sites are hydrographically linked in the modern ocean by vigorous circulation and the influence of Atlantic-derived waters across the Arctic Ocean[27]. The Holocene εNd at these three core sites are within error of modern compositions[29,30].

During the LGM the Yermak Plateau εNd averages to -13.1±0.9 (2σ (standard deviation) with a similar homogeneity and stability to the late Holocene but systematically offset in composition. The strong co-variation between these sites and

187 the homogeneous LGM and Holocene compositions (Fig. 2C) indicates that these
188 sites are recording an advected seawater signature resulting from Atlantic inflow and
189 deep-water mixing and not localised sediment inputs or pore fluid processes. While
190 some mixing with fresh and intermediate waters and localized inputs of Nd from
191 sediment may change the NAC εNd along its pathway, the homogeneity of the
192 signature at the LGM supports deep-water mixing that dominates over any local
193 process. The LGM εNd at the Yermak Plateau is within error of modern composition
194 of the NAC as it enters the Nordic Seas (-12.9±1.1 (2σ (standard deviation)[31]),
195 suggesting that this signature might be derived entirely from Atlantic waters.
196 However, the past NAC endmember composition is unknown, and it may well have
197 changed. The similar standard deviation of LGM εNd (Fig 2c) as the modern,
198 regardless of the absolute value, over several residence times of Nd in the ocean,
199 implies that at least the shallow site records the LGM NAC composition entering the
200 Arctic Ocean, and that the deeper sites reflect deep-water mixing of this signature. In
201 addition to previous evidence for the influence of Atlantic waters at the Yermak
202 Plateau during the LGM[12], these core sites indicate that authigenic εNd records an
203 active NAC inflow as well as transfer of these waters to depth at the Yermak Plateau
204 during the LGM.
205
206 **Last glacial maximum homogeneity**
207
208 The LGM Yermak Plateau εNd is similar to the rest of the Nordic Seas data (Fig. 1,
209 4). LGM compositions from this region approximate to a normal distribution (Fig. 4,
210 Methods) with a standard deviation similar to the late Holocene and modern
211 seawater, suggesting that there was a common water source at these sites at

212 different time periods. Therefore, the core sites were hydrographically connected
213 during the LGM. The link between the NAC at the Yermak Plateau and the deep
214 Nordic Seas indicates that there was widespread transformation of Atlantic waters to
215 depth. Our LGM data, therefore, indicates the influence of the Atlantic-derived waters
216 at the Nordic Seas and Yermak Plateau sites. The temperature over much of the
217 deep to intermediate Nordic Seas during the LGM was ~1 to 2°C warmer than the
218 modern[11,13], suggesting a lower net of cooling of high salinity NAC waters and a
219 reduced heat release to the atmosphere. Although more recent evidence suggests
220 there were periodically cooler bottom water temperatures during the LGM in the
221 Nordic Seas (e.g., near Svalbard[18,20]), which may reflect periodic and localized
222 higher efficiency cooling. We infer that the overall efficiency of surface to deep water
223 transformation was likely less than it is today, with moderately ventilated overflows
224 and deep waters[16,32]. Homogeneous Nordic Seas LGM εNd is interpreted as
225 evidence for deep-water formation. Our interpretation is that this deep-water
226 formation was probably a mixture of processes which are likely to have been
227 temporally variant. It is important to note that these findings represent time-
228 integrated averages and, therefore, show the continued dominant advective control
229 on εNd over thousands of years, despite highly variable sea-surface and sea-ice
230 conditions[25]. The homogeneity of seawater εNd compositions in this region show
231 that they were not locally changed by significant ice-rafted or other local sediment or
232 benthic inputs during the LGM, as potential source compositions are large[e.g.,22,33].
233
234 The processes affecting εNd in this region during the deglacial were different to both
235 the modern and LGM (Fig. 4). In contrast to the narrow normally distributed εNd
236 during the modern and LGM there is a wide (standard deviation = 4.4, Fig. 4) non-

normal (Methods, Extended Data Fig. 5 and Table 1) distribution during the deglaciation, suggesting that local Nd inputs with highly variable εNd dominated the sources of Nd, outcompeting homogenisation by deep-water mixing. Although there is consistency in the shift seen between some sites (Yermak Plateau, Central Norwegian Sea, Fig. 2), other sites show disparate compositions (Fig. 2, Fig. 4). The reason for this change may be a result of a mixture of two indistinguishable processes: firstly, an increased sedimentary and freshwater input of Nd with variable compositions into the basin and, secondly, a decrease or shutdown of deep-water formation processes, which both lead to a dominance of localised sources of Nd at several sites.

Connectivity to the Atlantic

Our data provide evidence for vigorous homogenisation of Nd throughout the water column leading to the conclusion that LGM deep-water was widespread across the central and eastern Nordic Seas and Yermak Plateau. Such widespread deep-water coupled with previous observations of moderately ventilated overflows to the east of Iceland[16] means that this deep-water was exported to the Atlantic. However, since a similar signature to the Nordic Seas is not seen in the NE Atlantic (Figs. 2 and 3), non-conservative processes (changing seawater εNd via input of Nd sourced from local sediment) may mask the εNd record of export to the NE Atlantic[24,34]. This dense water could also have exited the Nordic Seas via the Denmark Strait, as has been previously suggested[18,35]; however, no suitable εNd records have yet been obtained from the Denmark Strait.

It is possible that the deep-water formed in the Nordic Seas ventilated parts of the deep Atlantic, explaining previous observations of northern-sourced bottom water in the NW Atlantic[6,36,37]. Conceivably the Nordic Seas may have been the source of the ventilated dense water mass at 5 km depth observed in the NW Atlantic by Keigwin and Swift[6] and not the Labrador Sea as previously suggested.

These findings are of importance to the ongoing debate on the structure and nature of glacial-interglacial changes in Atlantic overturning and its link to climate, as it suggests that the Nordic Seas remained a critical source of dense water to the Atlantic during the LGM. Our dataset provides a benchmark for future AMOC modelling studies that use earth system models with Nd isotopes and infer LGM changes in the strength of deep-water formation in the Nordic Seas. The evidence presented herein indicates that LGM deep-water formation in the Nordic Seas was relatively widespread, and that deep-water mixing was vigorous enough to outcompete and homogenise other sources of Nd, rather than being confined to localised small scale processes.

Acknowledgments

C.S.L. thanks T. Williams, V. Rennie, R. Wang and M-L. Bagard, J. Hall, S. Crowhurst, G. Dipre and H. Chapman for assistance in the lab. C.S.L. is grateful to K. Hogan and C. Xuan for suggesting core locations. The British Ocean Sediment Core Research Facility, the Byrd Polar and Climate Research Center, Lamont-Doherty Core Repository and International Ocean Discovery Program are thanked for supplying sediment samples used in this study. C.S.L was funded by a NERC studentship (NE/L002507/1), with support from Murray Edwards College and the Geological Society's Elspeth Matthews Fund. Radiocarbon analysis was supported

by NERC Radiocarbon Facility NRCF010001 to A.M.P, S.G.M and C.S.L (allocation number 2117.0418). MME is funded by the Research Council of Norway and the Co-funding of Regional, National, and International Programmes (COFUND) – Marie Sklodowska-Curie Actions under the EU Seventh Framework Programme (FP7), project number 274429, and the Tromsø Research Foundation, project number A31720. MME and TLR received funding from the Research Council of Norway through its Centres of Excellence funding scheme, grant number 223259.

Author Contributions

The research was planned by C.S.L, A.M.P, E.T.T., with input from all authors. Analysis was carried out by C.S.L, apart from as follows: data from core PS1243 was obtained by N.L.R. Materials were supplied by H.A.B, R.F.S, L.P, T.L.R, M.S, R.N and M.M.E. The manuscript was written by C.S.L. with comments and contributions from all authors.

Competing Interests

The authors declare no competing interests.

Correspondence and requests for materials should be addressed to C.S.L (c.s.larkin@soton.ac.uk).

Figure Captions

Fig. 1. Deep-sea sediment core locations. **a**, Map showing core sites: red squares (records) and circles (core tops) measured in this study, blue diamonds are literature data[22,24,33,38–40]. Crossed blue circles represent sites of convection. Orange arrows

show near surface/intermediate currents: North Atlantic Current (NAC), East Greenland Current (EGC); blue arrows show deep currents: Arctic Intermediate Water (AIW), Denmark Strait Overflow Water (DSOW), Iceland-Scotland Overflow Water (ISOW), Wyville-Thomson Ridge Overflow Water (WTROW), Labrador Sea Water (LSW), North Atlantic Deep Water (NADW). The approximate extent of ice sheets (blue dashed line[41]) and the Arctic Ocean at the LGM (black dashed line[42]) are shown. Grey arrows represent the modern water inputs: major rivers, the Greenland ice-sheet, and Pacific derived water (PDW)[29]. **b**, Cross section. NAC flows into the eastern Nordic Seas (orange arrow), where convection occurs (light blue arrows). Deepwater flow (dark blue arrow) feeds into NADW (grey crossed circle indicates westward flow). Made using Ocean Data View (ODV)[43].

Fig. 2. Arctic Ocean, Nordic Seas and NE Atlantic neodymium isotope reconstructions over the last 35 ka. a, Map of core locations: diamonds, literature data; squares, this study. Colours match symbols for records in B-G. **b,** Arctic Ocean εNd: purple circles, Laptev Sea; white circles, Lomonosov Ridge[39]; black circles, Mendeleev Ridge[40]. **c**, Yermak Plateau εNd: yellow, dark blue, and light blue. **d,** Northern Norwegian Sea εNd[22]. **e,** Central Norwegian Sea: εNd, dark blue (this study); light blue[22]. **f**, Eastern Norwegian Sea εNd: purple and pink, Vøring Plateau; orange, Lofoten Basin. **g,** Greenland Sea εNd. **h,** NE Atlantic mixed planktic foraminifera: grayscale lines[24,38]. **i**, North Greenland ice core $\delta^{18}O$[44], YD: Younger Dryas, HS1–3: Heinrich Stadials 1–3, blue bars indicate these intervals. Orange box is the modern NAC composition entering the Nordic Seas[31]. **b-f,** circles are sediment leachates, squares are foraminifera. Typical 2σ (standard deviation) εNd errors are smaller or equal to the symbol size.

Fig. 3 Time-slice reconstructions of Arctic Ocean, Nordic Seas and North East Atlantic εNd. **a**, Modern seawater εNd[29–31,45–50]. **b,** Core top/late Holocene authigenic εNd. **c**, Time-slice authigenic εNd average during the LGM, 23–18 ka, grey dots in **a-c** are locations of data points (core sites and modern seawater sampling). **d**, Map showing location of cross section (X-Y, black dashed line), maximum extent of data used in εNd profiles (red line), and locations of data points (blue dots, core sites and modern seawater locations). Figure was created with ODV. White boxes indicate areas with a lack of data. Data used in b and c is summarised in Supplementary Table S7.

Fig. 4. Histogram and probability distribution of Nordic Seas and Yermak Plateau εNd. Data is split into 5 ka time intervals: late Holocene (5–0 ka, light red, data from 14 different core sites), deglacial (18–13 ka, orange, data from 10 different core sites), LGM (23–18 ka, blue, data from 12 different core sites). Modern seawater compositions over the same depth and latitudinal range as core sites (i.e., excluding near-surface seawater data) are also shown[29,31,46] (dark red). Bin-width is 1 epsilon unit and dashed lines indicate the means. Mean of the deglacial range is not shown. Authigenic εNd data includes data from this study, Maccali *et al.*[33] and, Struve *et al.*[22]. Means and associated 2σ errors are given.

References

1. Aagaard K., Swift J. H. & Carmack E. C. Thermohaline circulation in the Arctic Mediterranean Seas. *J. Geophys. Res. Oceans* **90**, 4833–4846 (1985).
2. Hansen, B. & Østerhus, S. North Atlantic–Nordic Seas exchanges. *Prog. Oceanogr.* **45**, 109–208 (2000).

3. Rahmstorf, S. Ocean circulation and climate during the past 120,000 years. *Nature* **419**, 207–214 (2002).

4. Howe, J. N. W. *et al.* North Atlantic Deep Water Production during the Last Glacial Maximum. *Nat. Commun.* **7**, 11765 (2016).

5. Oppo, D. W. *et al.* Data Constraints on Glacial Atlantic Water Mass Geometry and Properties. *Paleoceanogr. Paleoclimatology* **33**, 1013–1034 (2018).

6. Keigwin, L. D. & Swift, S. A. Carbon isotope evidence for a northern source of deep water in the glacial western North Atlantic. *Proc. Natl. Acad. Sci.* **114**, 2831–2835 (2017).

7. Ezat, M. M., Rasmussen, T. L., Skinner, L. C. & Zamelczyk, K. Deep ocean 14C ventilation age reconstructions from the Arctic Mediterranean reassessed. *Earth Planet. Sci. Lett.* **518**, 67–75 (2019).

8. Veum, T., Jansen, E., Arnold, M., Beyer, I. & Duplessy, J.-C. Water mass exchange between the North Atlantic and the Norwegian Sea during the past 28,000 years. *Nature* **356**, 783 (1992).

9. Bauch, H. A. *et al.* A multiproxy reconstruction of the evolution of deep and surface waters in the subarctic Nordic seas over the last 30,000yr. *Quat. Sci. Rev.* **20**, 659–678 (2001).

10. Hoffmann, S. S., McManus, J. F., Curry, W. B. & Brown-Leger, L. S. Persistent export of ^{231}Pa from the deep central Arctic Ocean over the past 35,000 years. *Nature* **497**, 603–606 (2013).

11. Thornalley, D. J. R. *et al.* A warm and poorly ventilated deep Arctic Mediterranean during the last glacial period. *Science* **349**, 706–710 (2015).

12. Nørgaard-Pedersen, N. *et al.* Arctic Ocean during the Last Glacial Maximum: Atlantic and polar domains of surface water mass distribution and ice cover. *Paleoceanography* **18**, 1063 (2003).

13. Ezat, M. M., Rasmussen, T. L. & Groeneveld, J. Persistent intermediate water warming during cold stadials in the southeastern Nordic seas during the past 65 k.y. *Geology* **42**, 663–666 (2014).

14. Knies, J. *et al.* Nordic Seas polynyas and their role in preconditioning marine productivity during the Last Glacial Maximum. *Nat. Commun.* **9**, 1–10 (2018).

15. Yu, J., Elderfield, H. & Piotrowski, A. M. Seawater carbonate ion-δ13C systematics and application to glacial–interglacial North Atlantic ocean circulation. *Earth Planet. Sci. Lett.* **271**, 209–220 (2008).

16. Ezat, M. M. *et al.* Ventilation history of Nordic Seas overflows during the last (de)glacial period revealed by species-specific benthic foraminiferal 14C dates. *Paleoceanography* **32**, 172–181 (2017).

17. Cronin, T. M. *et al.* Deep Arctic Ocean warming during the last glacial cycle. *Nat. Geosci.* **5**, 631–634 (2012).

18. Ezat, M. M. *et al.* Deep Ocean Storage of Heat and CO2 in the Fram Strait, Arctic Ocean During the Last Glacial Period. *Paleoceanogr. Paleoclimatology* **36**, e2021PA004216 (2021).

19. Rasmussen, T. L. & Thomsen, E. Warm Atlantic surface water inflow to the Nordic seas 34–10 calibrated ka B.P. *Paleoceanography* **23**, (2008).

20. Altuna, N. E. bani, Ezat, M. M., Greaves, M. & Rasmussen, T. L. Millennial-Scale Changes in Bottom Water Temperature and Water Mass Exchange Through the Fram Strait 79°N, 63-13 ka. *Paleoceanogr. Paleoclimatology* **36**, e2020PA004061 (2021).

21. Frank, M. Radiogenic isotopes: Tracers of past ocean circulation and erosional input. *Rev. Geophys.* **40**, (2002).
22. Struve, T. *et al.* Ice-sheet driven weathering input and water mass mixing in the Nordic Seas during the last 25,000 years. *Earth Planet. Sci. Lett.* **514**, 108–118 (2019).
23. Abbott, A. N. A benthic flux from calcareous sediments results in non-conservative neodymium behavior during lateral transport: A study from the Tasman Sea. *Geology* **47**, 363–366 (2019).
24. Roberts, N. L. & Piotrowski, A. M. Radiogenic Nd isotope labeling of the northern NE Atlantic during MIS 2. *Earth Planet. Sci. Lett.* **423**, 125–133 (2015).
25. Müller, J. & Stein, R. High-resolution record of late glacial and deglacial sea ice changes in Fram Strait corroborates ice–ocean interactions during abrupt climate shifts. *Earth Planet. Sci. Lett.* **403**, 446–455 (2014).
26. Chauhan, T., Rasmussen, T. L. & Noormets, R. Palaeoceanography of the Barents Sea continental margin, north of Nordaustlandet, Svalbard, during the last 74 ka. *Boreas* **45**, 76–99 (2016).
27. Rudels, B. *et al.* The interaction between waters from the Arctic Ocean and the Nordic Seas north of Fram Strait and along the East Greenland Current: results from the Arctic Ocean-02 Oden expedition. *J. Mar. Syst.* **55**, 1–30 (2005).
28. Chauhan, T., Noormets, R. & Rasmussen, T. L. Glaciomarine sedimentation and bottom current activity on the north-western and northern continental margins of Svalbard during the late Quaternary. *Geo-Mar. Lett.* **36**, 81–99 (2016).
29. Laukert, G. *et al.* Ocean circulation and freshwater pathways in the Arctic Mediterranean based on a combined Nd isotope, REE and oxygen isotope section across Fram Strait. *Geochim. Cosmochim. Acta* **202**, 285–309 (2017).

30. Andersson, P. S. *et al.* Neodymium isotopes in seawater from the Barents Sea and Fram Strait Arctic–Atlantic gateways. *Geochim. Cosmochim. Acta* **72**, 2854–2867 (2008).

31. Lacan, F. & Jeandel, C. Neodymium isotopic composition and rare earth element concentrations in the deep and intermediate Nordic Seas: Constraints on the Iceland Scotland Overflow Water signature. *Geochem. Geophys. Geosystems* **5**, Q11006 (2004).

32. Telesiński, M. M., Ezat, M. M., Muschitiello, F., Bauch, H. A. & Spielhagen, R. F. Ventilation History of the Nordic Seas Deduced From Pelagic-Benthic Radiocarbon Age Offsets. *Geochem. Geophys. Geosystems* **22**, e2020GC009132 (2021).

33. Maccali, J., Hillaire-Marcel, C., Carignan, J. & Reisberg, L. C. Geochemical signatures of sediments documenting Arctic sea-ice and water mass export through Fram Strait since the Last Glacial Maximum. *Quat. Sci. Rev.* **64**, 136–151 (2013).

34. Vogt-Vincent, N., Lippold, J., Kaboth-Bahr, S. & Blaser, P. Ice-rafted debris as a source of non-conservative behaviour for the εNd palaeotracer: insights from a simple model. *Geo-Mar. Lett.* (2020) doi:10.1007/s00367-020-00643-x.

35. Millo, C., Sarnthein, M., Voelker, A. & Erlenkeuser, H. Variability of the Denmark Strait Overflow during the Last Glacial Maximum. *Boreas* **35**, 50–60 (2006).

36. Pöppelmeier, F. *et al.* Influence of Ocean Circulation and Benthic Exchange on Deep Northwest Atlantic Nd Isotope Records During the Past 30,000 Years. *Geochem. Geophys. Geosystems* **20**, 4457–4469 (2019).

37. Blaser, P. *et al.* Labrador Sea bottom water provenance and REE exchange during the past 35,000 years. *Earth Planet. Sci. Lett.* **542**, 116299 (2020).

38. Crocker, A. J. *et al.* Geochemical response of the mid-depth Northeast Atlantic Ocean to freshwater input during Heinrich events 1 to 4. *Quat. Sci. Rev.* **151**, 236–254 (2016).

39. Haley, B. A., Frank, M., Spielhagen, R. F. & Eisenhauer, A. Influence of brine formation on Arctic Ocean circulation over the past 15 million years. *Nat. Geosci.* **1**, 68–72 (2008).

40. Jang, K. *et al.* Glacial freshwater discharge events recorded by authigenic neodymium isotopes in sediments from the Mendeleev Ridge, western Arctic Ocean. *Earth Planet. Sci. Lett.* **369–370**, 148–157 (2013).

41. Spielhagen, R. Glaciology: Enigmatic Arctic ice sheets. *Nature* **410**, 427–428 (2001).

42. Clark, P. U. *et al.* The Last Glacial Maximum. *Science* **325**, 710–714 (2009).

43. Schlitzer, R. Ocean Data View, odv.awi.de, (2021).

44. NGRIP Project Members. High-resolution record of Northern Hemisphere climate extending into the last interglacial period. *Nature* **431**, 147 (2004).

45. Dubois-Dauphin, Q. *et al.* Fingerprinting Northeast Atlantic water masses using neodymium isotopes. *Geochim. Cosmochim. Acta* **210**, 267–288 (2017).

46. Lacan, F. & Jeandel, C. Subpolar Mode Water formation traced by neodymium isotopic composition. *Geophys. Res. Lett.* **31**, (2004).

47. Laukert, G. *et al.* Transport and transformation of riverine neodymium isotope and rare earth element signatures in high latitude estuaries: A case study from the Laptev Sea. *Earth Planet. Sci. Lett.* **477**, 205–217 (2017).

48. Werner, K., Frank, M., Teschner, C., Müller, J. & Spielhagen, R. F. Neoglacial change in deep water exchange and increase of sea-ice transport through eastern Fram Strait: evidence from radiogenic isotopes. *Quat. Sci. Rev.* **92**, 190–207 (2014).

49. Zimmermann, B. *et al.* Hafnium isotopes in Arctic Ocean water. *Geochim. Cosmochim. Acta* **73**, 3218–3233 (2009).

50. Porcelli, D. *et al.* The distribution of neodymium isotopes in Arctic Ocean basins. *Geochim. Cosmochim. Acta* **73**, 2645–2659 (2009).

Methods

Deep-sea sediment cores used in this study were obtained as listed in the Supplementary Table S1.

Authigenic neodymium isotopes. Authigenic Nd isotopes were measured on either sediment leachates and/or mixed species of planktic foraminifera. Mixed planktic foraminifera were not reductively cleaned but had clay particles removed following[24] and references therein. In short, mixed planktic foraminifera were picked from the coarse fraction (> 63 μm) and then crushed between two glass plates, rinsed, sonicated and any clays removed. The samples were then dissolved in 1M glacial acetic acid.

Marine sediment was leached with a weak acid-reductive leach in order to extract the seawater-derived hydrogenic ferromanganese (oxy)hydroxide phases following the significantly improved method of Blaser *et al.*[51]. In brief, a 5mM hydroxylamine hydrochloride-3mM Na-EDTA-1.5% acetic acid leach buffered to a pH of ~4 with

NaOH was reacted with dry sediment. The following modifications from Blaser *et al.*[51] were made: 1–2 g of sediment was leached in 10 mls of reagent instead of 0.3–0.4 g, and the reaction time was reduced to 20–30 minutes. These modifications improved the sample/reagent ratio and reduced even further the likelihood of leaching into the detrital fraction[52]. Unless otherwise stated, sediment leaches were carried out on bulk sediment. A small number of sediment leaches were carried out on the fine fraction (<63 μm) in addition to the bulk, as noted in Supplementary Table S4. There was no significant difference between bulk sediment leachates and fine fraction leachates carried out at the same depth, as both agree within uncertainty. Nd was extracted using established ion-exchange chromatographic procedures: rare earth elements were extracted using TRUspec resin, and Nd was then separated from the other rare earth elements using Eichrom LNspec resin[4]. Neodymium isotopes where measured on a Thermo Fischer Neptune Plus MC-ICP-MS at the University of Cambridge Department of Earth Sciences, apart from mixed planktic foraminifera from core PS1243, which were measured on a Nu Plasma HR-MC-ICP-MS. $^{146}Nd/^{144}Nd$ was normalised to 0.7219, and samples were run with a concentration-matched solution of reference standard JNdi-1 and were corrected to the accepted value of JNdi-1: $^{143}Nd/^{144}Nd=0.512115$[53]. The εNd of each sample is quoted alongside the external error (2σ) (Supplementary Tables S4), which is 2 times the standard deviation on replicate measurements of the concentration matched JNdi-1 reference standard across the corresponding measurement session (typically 6–12 hours long). εNd was calculated in parts per 10,000 relative to the chondritic uniform reservoir, $^{143}Nd/^{144}NdCHUR=0.512638$[54]. Longer-term external and internal reproducibility was monitored using digested US Geological Survey (USGS) rock standards, with a least one standard analysed per analytical session

and standards being regularly passed through column chemistry at the same time as samples. Rock standards measured were as follows: BHVO-2 εNd=6.78±0.17 (2σ), n=14, BCR-2 εNd=-0.1±0.26 (2σ), n=14, SCO-1 εNd=-10.48±0.27 (2σ), n=8. All 3 rock standards are within error of previously published values: BHVO-2 εNd=6.75±0.21 (2σ), BCR-2 εNd=-0.02±0.23 (2σ)[55], SCO-1 εNd =-10.77±0.57 (2σ)[56]. Full procedural replicates reproduced values within uncertainty.

3 full procedural (2 leachates, and one foraminifera) and 2 column chemistry blanks were determined by isotope dilution using either a ^{150}Nd or ^{146}Nd spike measured on either a TIMS VG Sector 54 in ion counting mode or a Neptune Plus MC-ICP-MS. Samples were not blank corrected as blanks ranged from 6–26 pg, representing ≤0.5% of all sample sizes analysed.

Reliability of bulk sediment leachates. The reliability of bulk sediment leachates as tracers of past seawater εNd was tested by comparing core top values to those of modern seawater compositions and foraminifera measured at the same core depth. Core top values are closely correlated with the closest published seawater value. Seawater values alongside core top measurements are summarised in Extended Data Fig. 1. Foraminiferal εNd and bulk sediment leachates from the same depth are compared in Extended Data Fig. 1. Both foraminiferal and bulk sediment leachates values are in close agreement over a wide range of εNd.

Concentrations of a suite of major and some trace elements were monitored in several of the sediment leachates (across a wide range of εNd compositions) in order to check for detrital contamination following Blaser *et al.*[51]. Leachate samples were measured using a matrix-matched calibration line made of single elemental

557 standards on an Agilent Technologies ICP-OES in the Department of Earth
558 Sciences, University of Cambridge. External reproducibility was monitored using
559 certified standards SPS-SW2 (Spectrapure Standards AS, Oslo, Norway) and a
560 digested USGS rock standard BCR-2, diluted with a matrix matched blank leach
561 solution; values obtained with their deviation from certified values are summarised in
562 Supplementary Table S2. Nd concentrations < ~ 2ppb were below detection, and
563 samples were analysed at > 4 ppb Nd. A mixture of single element standards was
564 used to monitor instrumental drift. The ratios of Al/Nd and Sr/Ca were calculated and
565 compared to the normal 'hydrogenic' range as defined by[51,57] (Sr/Ca (mg/g) > 2,
566 Al/Nd (g/g) ~ < 110), none of the leachates analysed fell significantly outside this
567 range suggesting no significant detrital contamination (Supplementary Table S3).
568
569 **Age Models.** Existing published age models used in this study are summarised in
570 Supplementary Table 5.
571
572 Core GIK23074 is tied to the Lake Suigetsu record using ^{14}C plateau tuning[58] and is
573 put on the U-Th model age timescale of Bronk Ramsey *et al.*[59] in calendar years
574 before present (BP). Age models from the Nordic Seas and Arctic Ocean reliant on
575 radiocarbon dating were recalculated using the Marine13 calibration, since the
576 Marine20 data set is not considered suitable for samples from polar regions[60], with
577 Bayesian Age-Depth Modelling software 'BACON' v.2.3.3 in R[61] (Extended Data Fig.
578 2, supplementary Table S5) with appropriate surface reservoir age corrections
579 (supplementary Table S5). The maximum and minimum ages shown in
580 supplementary data tables are the 95% confidence intervals. The age used is the
581 mean age and is given in calendar years before present. Several cores with more

poorly constrained age models[62–64] were selected for time slice (LGM and Holocene) measurements only, as outlined in supplementary Table S1.

Radiocarbon ages were obtained for HLY0503-22-TC and PS2212-3 on mixed planktic foraminifera (N. *pachyderma*, T. *quinqueloba*) picked from the > 63 μm fraction. Preparation of samples was carried out with the assistance of technical staff at the NERC Radiocarbon Facility. The outer 20% (by weight) of shell was removed by controlled hydrolysis with dilute HCl. The samples were then rinsed in deionised water, dried, and homogenised. A known weight of the sample was hydrolysed to CO_2 using 85% orthophosphoric acid at room temperature. The CO_2 was converted to graphite by Fe/Zn reduction. $\delta^{13}C$ was measured on a dual inlet stable isotope mass spectrometer (Thermo Fisher Delta V). Radiocarbon ages were obtained by technical staff at the Scottish Universities Environmental Research Centre accelerator mass spectrometer (AMS). One low mass sample (0.337 mg carbon) was obtained by technical staff at the Keck Carbon Cycle AMS Facility, University of California, Irvine. Radiocarbon ages obtained are summarised in Supplementary Table S6. These uncalibrated radiocarbon ages were input into 'BACON' Bayesian Age-Depth Modelling software in R[61] where they were calibrated automatically using the Marine13 calibration. An appropriate surface ocean reservoir age correction was also input for each date[58,65] and is summarised in Supplementary Table S6. Additional tie points were also included: HLY0503-22-TC was tied to the previously dated piston core deployed at the same time (HLY0503-22-JPC[66]) using magnetic susceptibility, and PS2212-3 was tied to nearby dated cores using a synchronous mineralogical event—Event I—characterised by the presence of ordered-layered expandable minerals (OLEM)[67]. The synthesised age scale produced using

607 ‘BACON’, which takes into consideration the error in the radiocarbon calibration, is
608 shown alongside new εNd data in the supplementary data tables. The age taken is
609 the mean, and the 95% confidence interval is shown as the maximum and minimum
610 age.
611
612 Core PS1243 has been tied to records from the southern Norwegian Sea, which
613 have been tied to the North Greenland Ice Core Project (NGRIP), based upon
614 planktic $\delta^{18}O$[11].The εNd data from Struve *et al.*[22] has been put on the slightly
615 modified age scale of core PS1243 from Ezat *et al.*[16], in which PS1243 was aligned
616 to core JM11-FI-19PC using planktic $\delta^{18}O$. The independent chronology of JM11-FI-
617 19PC is based on several proxy alignments to Greenland ice cores in addition to
618 tephra layers that are common to Greenland ice cores. PS1243 has been placed on
619 the Greenland Ice Core Chronology 2005 time scale (GICC05[68]), and ages have
620 been converted from b2k to years BP.
621
622 The age model originally used for core JM06-WP-16-MC[33] in the western Fram Strait
623 relied on radiocarbon ages, and the authors did not make any assumption about
624 surface reservoir age when constructing the age model. Surface reservoir ages in
625 this region are likely to have been variable and potentially very large, particularly
626 during the deglaciation[11,58]. In order to make this record comparable with the
627 timescales used in this study, the radiocarbon ages are recalibrated with reasonable
628 surface reservoir age corrections from Thornalley *et al.*[11], and the age depth model
629 is reconstructed using ‘BACON’ in the same way as for new and recalculated age-
630 depth scales for new data presented in this study. This recalculation shifts data
631 points which were originally considered to be LGM in age to substantially younger

ages. These data points are now deglacial (< 18 ka) in age, and the record is, therefore, directly comparable with other records in this study. The rest of the age models used for literature data are the same as in the original papers[22,24,38].

These differing methods for obtaining age models are comparable over the time scales of interest (on the order of several hundreds to thousands of years) because of the similarity in the planktic $\delta^{18}O$ records[9,13,69–72] (Extended Data Fig. 3). However, differing resolutions in and types of age models mean that not all records may necessarily be directly comparable on centennial timescales. There is likely to be unknown uncertainty that is not necessarily covered by the bayesian age-depth modelling approach. Above all, marine reservoir ages are likely to have been significant and variable over the timescale of interest, and although some assumptions are made based on several previous studies to ensure comparability, these assumptions have unknown and large errors. For this reason, the whole dataset is considered primarily as averages over 1000's of years, rather than comparing smaller scale temporal shifts. Despite these shortcomings, the dataset resolution is sufficient to enable comparisons over the timescales of interest.

Synthesis and statistical analysis. Deep-sea sediment core sites were chosen for higher resolution records based upon the presence of existing well-defined age models and/or high sedimentation rates. A series of core sites were analysed only for their core top compositions (Fig.1, supplementary table S1) to compare with modern seawater compositions. Several cores with lower-resolution age models were analysed only at the LGM and Holocene. New εNd measurements were obtained primarily from weak acid-reductive sediment leaches, with additional

657 measurements on non-chemically cleaned mixed planktic foraminifera where
658 possible, from this wide range of sediment core sites in the Arctic Ocean and Nordic
659 Seas (supplementary table S1). The new εNd records are combined with three
660 published records from the Nordic Seas for analysis (Fig. 4). To understand the
661 larger scale patterns of εNd in this region, all data (including literature data) north of
662 the GSR in the Nordic Seas and at the Yermak Plateau (sites as shown in Extended
663 Data Fig. 4) are split into 3 equal time intervals, comprising the late Holocene (5-0
664 ka), the deglaciation (18-13 ka) and the LGM (23-18 ka). There is insufficient data
665 from too few core sites to adequately characterise the data in this manner > 23 ka.
666 The data is averaged and shown as probability density estimates and histograms
667 (Fig. 4). The late Holocene is compared with seawater values from the same depth
668 and latitudinal range as well as to the LGM and deglacial values. The late Holocene
669 data is within error of the modern seawater array. The LGM values average to a
670 composition which is systematically offset from the Late Holocene by between -2.7
671 and -2.2 epsilon units (95% confidence intervals), but with a similar spread (2σ =1.2
672 and 1.1 respectively). Although the deglacial average is within error of the Late
673 Holocene, values are disparate, and the spread is large (2σ =4.4).
674 Simple statistical tests were applied to the averaged datasets shown in Fig. 4 to
675 compare their distributions both in terms of absolute compositions and structure.
676 Means, variances, and distributions (normal/non-normal) were compared and
677 appropriate statistical tests carried out in R.
678
679 Kernel density estimates (probability distributions) shown in Fig. 4 show that the late
680 Holocene, seawater, and LGM datasets approximate to normal distributions. The
681 deglacial dataset, in comparison, forms a flattened distribution with a greater

682 standard deviation to the LGM, modern, and Holocene data. This deviation from the
683 normal distribution seen at the LGM and Holocene is not caused by sampling
684 limitations as the sample size is large (n=96).
685
686 The Shapiro-Wilk test of normality was applied to each of the εNd datasets
687 (Extended Data Table 1). If this test is significant (p-value < 0.05), the distribution is
688 non-normal. The late Holocene, seawater, and LGM arrays are all shown to be not
689 significantly different from a normal distribution. The deglacial data is confirmed to be
690 non-normally distributed. Quantile-quantile normal plots additionally indicated
691 normality (no significant departures from the 1:1 line as all points lie within the 95%
692 error envelope) for the late Holocene, seawater, and LGM datasets and indicated
693 significant departures from the 1:1 line for the deglacial dataset (Extended Data Fig.
694 5).
695
696 The variances of the distributions shown to be normal (modern seawater, late
697 Holocene, and LGM) with similar standard deviations (Fig. 4) are compared using an
698 F-test (Extended Data Table 2). This assesses whether the scatter (spread) in each
699 of these datasets is comparable. The F-test assesses the ratio of the variances of
700 two datasets. The closer to F=1 the more likely the data have equal population
701 variances. If the test is significant (p-value < 0.05), the two distributions have
702 differing variances. The LGM and Late Holocene datasets have similar variances.
703 This, combined with the Shapiro-Wilk test, implies similarity in both the width and the
704 type of distribution of these datasets, despite differing means (Fig. 4).
705

The late Holocene and modern seawater datasets have significantly different variances, and the seawater dataset has a lower standard deviation when compared to the Holocene (0.8 versus 1.1). This difference may be explained by an uneven geographical distribution of data points between the two datasets and a non-comparable timeframe (a 5000-year interval versus snapshots from the past two decades).

In summary, these statistical tests show that the modern seawater, late Holocene, and LGM datasets all form normal distributions. The late Holocene and LGM datasets have similar variances and so are indistinguishable in both width and type of distribution but differ in absolute composition. The deglacial dataset differs from all other datasets.

Constraints on past NAC εNd. The past NAC composition likely remained unradiogenic, as today surface to sub-surface εNd in the sub-polar N. Atlantic gyre are influenced by conservative mixing with very unradiogenic glacial and riverine inputs from N. America and Greenland, which is set by the unradiogenic bedrock composition of these regions[73]. Although surface water εNd tends to be much more variable, and affected by wind-blown inputs, strong advection in subsurface Atlantic waters in the modern sub-polar gyre also appear to lead to much more conservative εNd behavior[73].

Data availability: All data from this study can be found in the supplementary information (data tables) and can be accessed through the PANGAEA data archive.

Code availability: All modelling and statistical analysis was carried out with the use of published open-access software in R, as referenced in the methods. R codes used for the numerical procedures are available from the corresponding author upon reasonable request**.**

Methods-only references

51. Blaser, P. *et al.* Extracting foraminiferal seawater Nd isotope signatures from bulk deep sea sediment by chemical leaching. *Chem. Geol.* **439**, 189–204 (2016).

52. Wilson, D. J., Piotrowski, A. M., Galy, A. & Clegg, J. A. Reactivity of neodymium carriers in deep sea sediments: Implications for boundary exchange and paleoceanography. *Geochim. Cosmochim. Acta* **109**, 197–221 (2013).

53. Tanaka, T. *et al.* JNdi-1: a neodymium isotopic reference in consistency with LaJolla neodymium. *Chem. Geol.* **168**, 279–281 (2000).

54. Jacobsen, S. B. & Wasserburg, G. J. Sm-Nd isotopic evolution of chondrites. *Earth Planet. Sci. Lett.* **50**, 139–155 (1980).

55. Weis, D. *et al.* High-precision isotopic characterization of USGS reference materials by TIMS and MC-ICP-MS. *Geochem. Geophys. Geosystems* **7**, Q08006 (2006).

56. Hindshaw, R. S., Aciego, S. M., Piotrowski, A. M. & Tipper, E. T. Decoupling of dissolved and bedrock neodymium isotopes during sedimentary cycling. *Geochem. Perspect. Lett.* 43–46 (2018) doi:10.7185/geochemlet.1828.

57. Blaser, P. *et al.* The resilience and sensitivity of Northeast Atlantic deep water εNd to overprinting by detrital fluxes over the past 30,000 years. *Geochim. Cosmochim. Acta* **245**, 79–97 (2019).

58. Sarnthein, M., Balmer, S., Grootes, P. & Mudelsee, M. Planktic and Benthic 14C Reservoir Ages for Three Ocean Basins, Calibrated by a Suite of 14C Plateaus in the Glacial-to-Deglacial Suigetsu Atmospheric 14C Record. *Radiocarbon* **57**, 129–151 (2015).

59. Bronk Ramsey, C. *et al.* A Complete Terrestrial Radiocarbon Record for 11.2 to 52.8 kyr B.P. *Science* **338**, 370–374 (2012).

60. Heaton, T. J. *et al.* Marine20—The Marine Radiocarbon Age Calibration Curve (0–55,000 cal BP). *Radiocarbon* **62**, 779–820 (2020).

61. Blaauw, M. & Christen, J. A. Flexible paleoclimate age-depth models using an autoregressive gamma process. *Bayesian Anal.* **6**, 457–474 (2011).

62. *Proceedings of the Ocean Drilling Program, 104 Scientific Results*. vol. 104 (Ocean Drilling Program, 1989).

63. Stein, R. *et al.* Accumulation of particulate organic carbon at the Eurasian continental margin during late Quaternary times: controlling mechanisms and paleoenvironmental significance. *Glob. Planet. Change* **31**, 87–104 (2001).

64. Vogelsang, E., Sarnthein, M. & Pflaumann, U. d18O Stratigraphy, chronology, and sea surface temperatures of Atlantic sediment records (GLAMAP-2000 Kiel). *Berichte - Rep. Inst. Für Geowiss. Christ.-Albrechts-Univ. Kiel* (2001).

65. Mangerud, J. & Gulliksen, S. Apparent Radiocarbon Ages of recent marine shells from Norway, Spitsbergen, and Arctic Canada. *Quat. Res.* **5**, 263–273 (1975).

66. Xuan, C., Channell, J. E. T., Polyak, L. & Darby, D. A. Paleomagnetism of Quaternary sediments from Lomonosov Ridge and Yermak Plateau: implications for age models in the Arctic Ocean. *Quat. Sci. Rev.* **32**, 48–63 (2012).

67. Vogt, C., Knies, J., Spielhagen, R. F. & Stein, R. Detailed mineralogical evidence for two nearly identical glacial/deglacial cycles and Atlantic water advection to the Arctic Ocean during the last 90,000 years. *Glob. Planet. Change* **31**, 23–44 (2001).

68. Svensson, A. *et al.* A 60 000 year Greenland stratigraphic ice core chronology. *Clim. Past* **4**, 47–57 (2008).

69. Dokken, T. M. & Jansen, E. Rapid changes in the mechanism of ocean convection during the last glacial period. *Nature* **401**, 458–461 (1999).

70. Telesiński, M. M., Bauch, H. A., Spielhagen, R. F. & Kandiano, E. S. Evolution of the central Nordic Seas over the last 20 thousand years. *Quat. Sci. Rev.* **121**, 98–109 (2015).

71. Voelker, A. H. L. *et al.* Correlation of Marine 14C Ages from the Nordic Seas with the GISP2 Isotope Record: Implications for 14C Calibration Beyond 25 ka BP. *Radiocarbon* **40**, 517–534 (1997).

72. Weinelt, M. *et al.* Variability of North Atlantic heat transfer during MIS 2. *Paleoceanography* **18**, (2003).

73. Lambelet, M. *et al.* Neodymium isotopic composition and concentration in the western North Atlantic Ocean: Results from the GEOTRACES GA02 section. *Geochim. Cosmochim. Acta* **177**, 1–29 (2016).

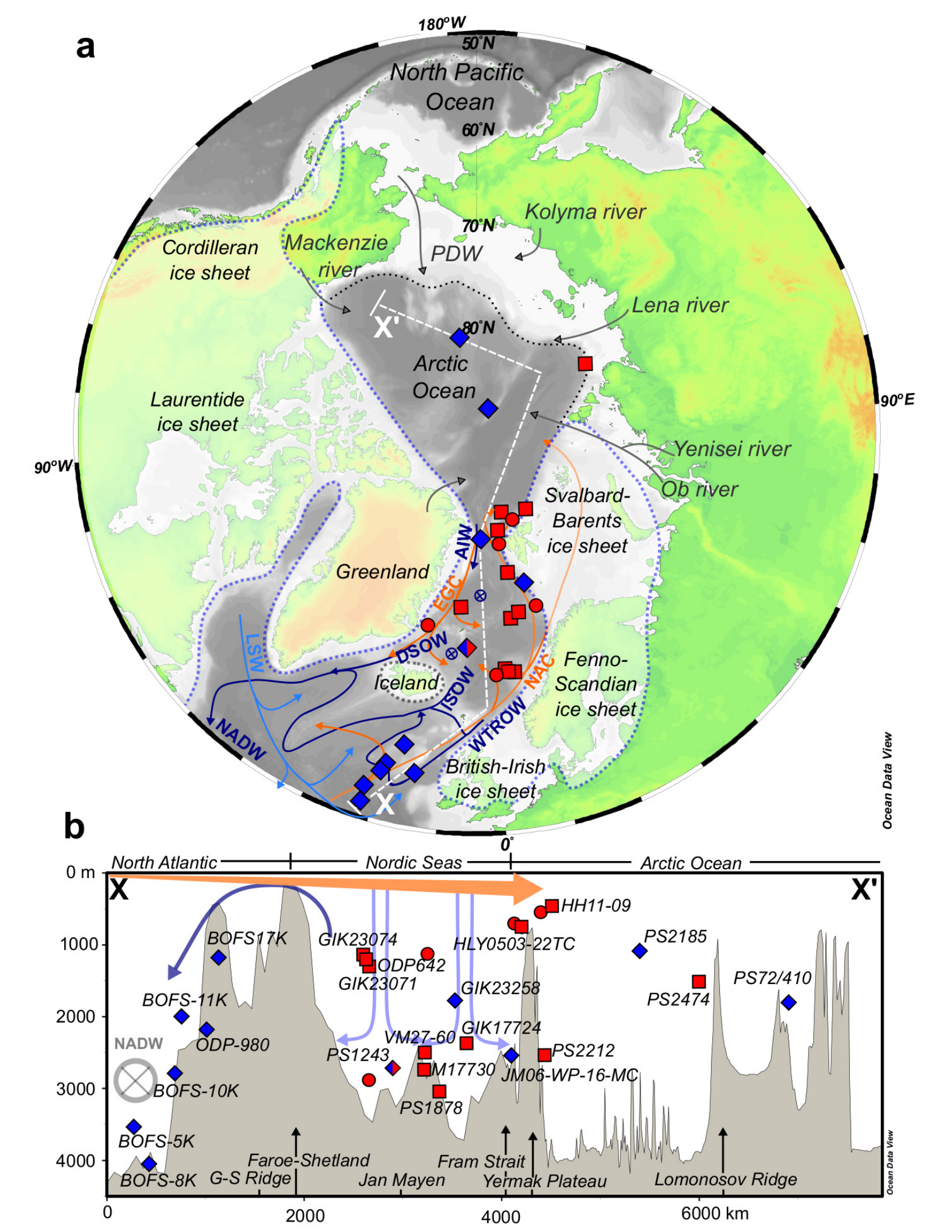
a
180°W
50°N
North Pacific Ocean
60°N
70°N
80°N
90°W
90°E
0°
Kolyma river
Mackenzie river
PDW
Cordilleran ice sheet
Lena river
X'
Arctic Ocean
Laurentide ice sheet
Yenisei river
Ob river
Svalbard-Barents ice sheet
Greenland
AIW
EGC
LSW
DSOW
ISOW
NAC
WTROW
NADW
Iceland
Fenno-Scandian ice sheet
British-Irish ice sheet
X
Ocean Data View
b
North Atlantic
Nordic Seas
Arctic Ocean
0 m
1000
2000
3000
4000
X
X'
HH11-09
BOFS17K
GIK23074
HLY0503-22TC
PS2185
ODP642
GIK23071
GIK23258
PS72/410
PS2474
BOFS-11K
NADW
ODP-980
VM27-60
GIK17724
PS1243
PS2212
M17730
JM06-WP-16-MC
BOFS-10K
PS1878
BOFS-5K
BOFS-8K
Faroe-Shetland G-S Ridge
Jan Mayen
Fram Strait
Yermak Plateau
Lomonosov Ridge
0
2000
4000
6000 km
Ocean Data View

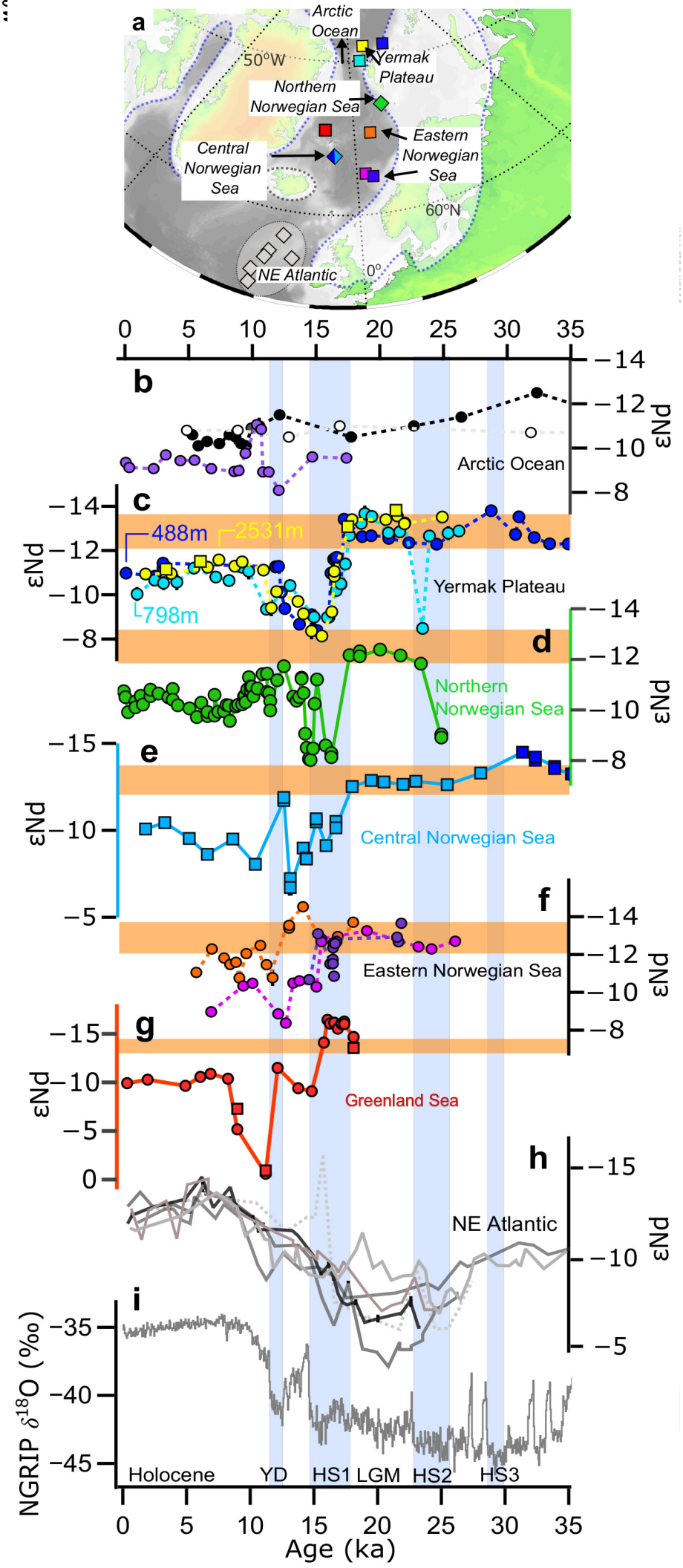
a
Arctic Ocean
50°W
Yermak Plateau
Northern Norwegian Sea
Central Norwegian Sea
Eastern Norwegian Sea
60°N
NE Atlantic
0°
0 5 10 15 20 25 30 35
b
Arctic Ocean
εNd
c
488m
531m
798m
Yermak Plateau
d
Northern Norwegian Sea
e
Central Norwegian Sea
f
Eastern Norwegian Sea
g
Greenland Sea
h
NE Atlantic
i
NGRIP δ18O (‰)
Holocene
YD
HS1
LGM
HS2
HS3
Age (ka)

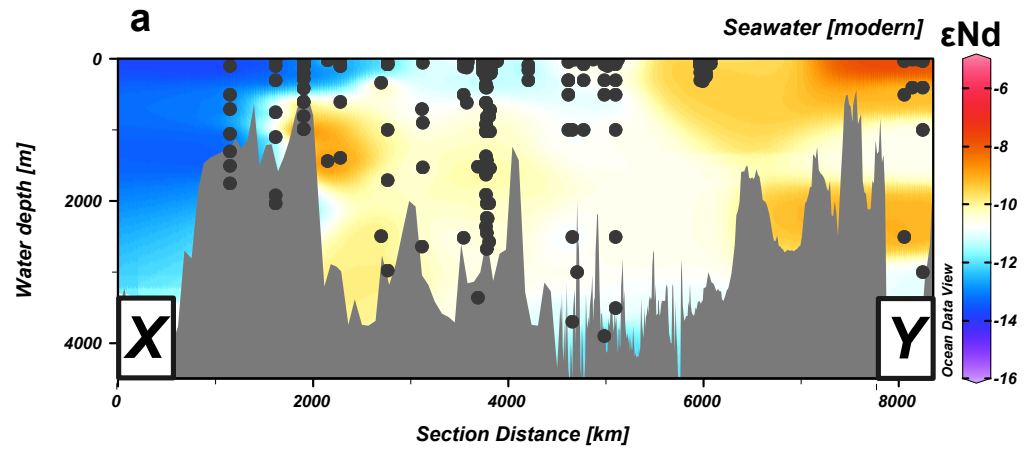
a
Seawater [modern]
εNd
Water depth [m]
0
2000
4000
X
Y
0
2000
4000
6000
8000
Section Distance [km]
Ocean Data View
-6
-8
-10
-12
-14
-16

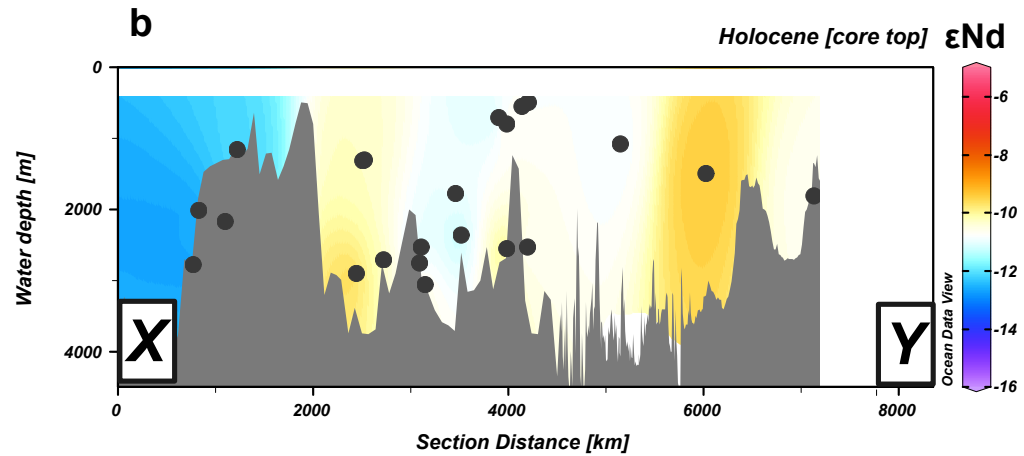
b
Holocene [core top]
εNd
Water depth [m]
0
2000
4000
X
Y
0
2000
4000
6000
8000
Section Distance [km]
Ocean Data View
-6
-8
-10
-12
-14
-16

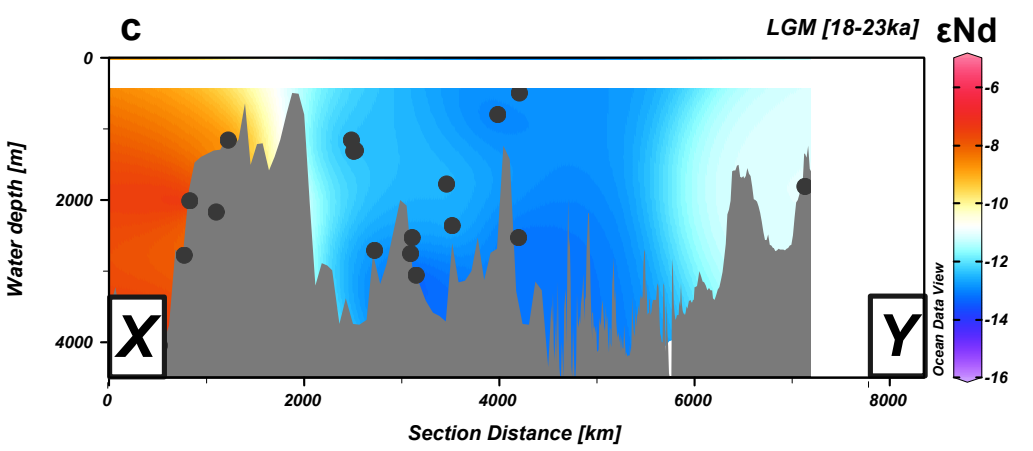
c
LGM [18-23ka]
εNd
Water depth [m]
0
2000
4000
X
Y
0
2000
4000
6000
8000
Section Distance [km]
Ocean Data View
-6
-8
-10
-12
-14
-16

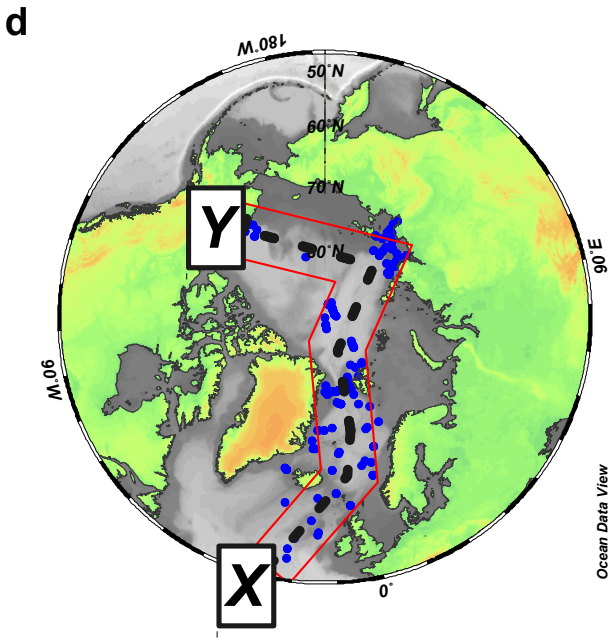
d
180°W
50°N
60°N
70°N
80°N
90°W
0°
90°E
Y
X
Ocean Data View

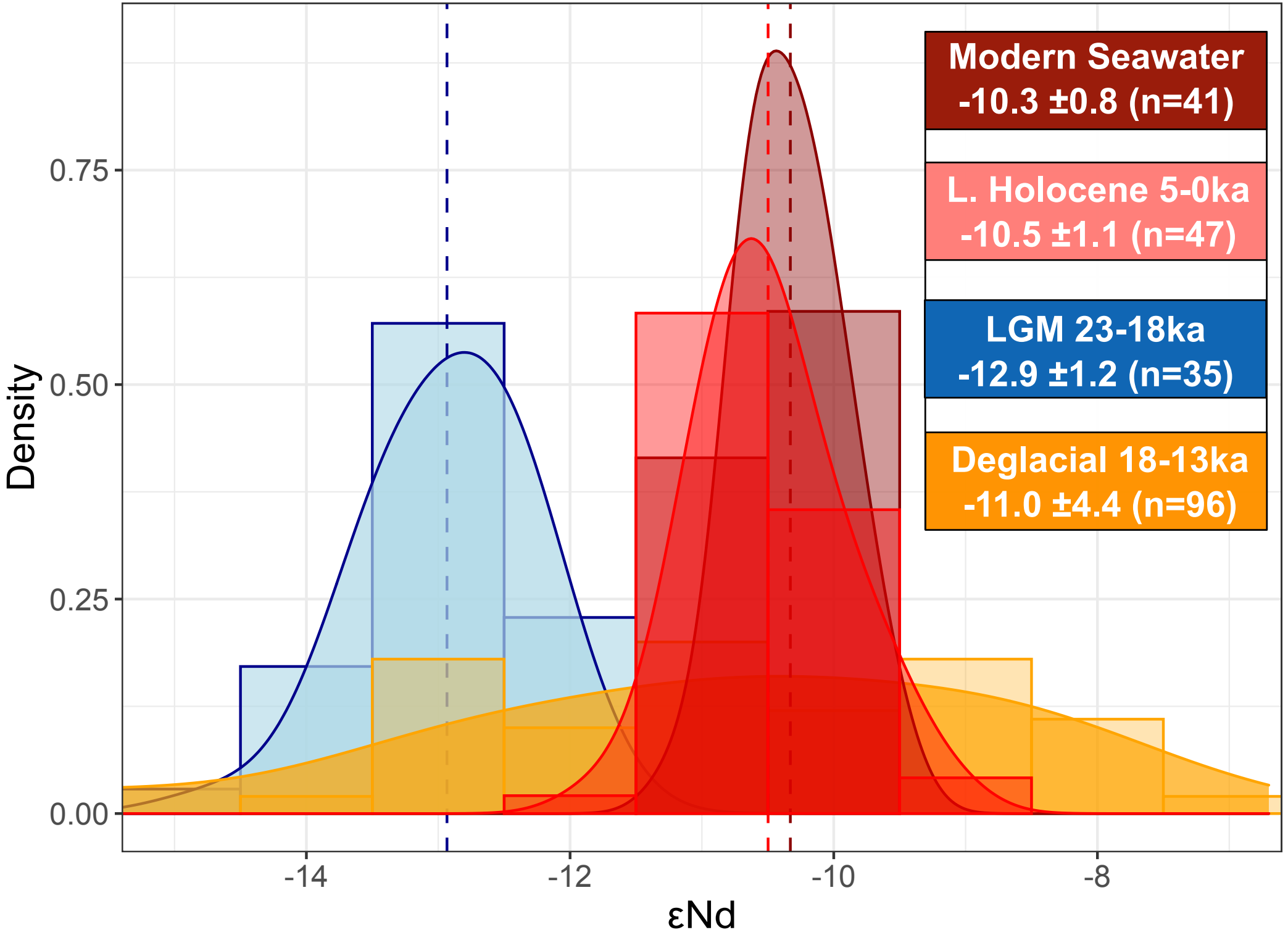
Modern Seawater
-10.3 ±0.8 (n=41)
L. Holocene 5-0ka
-10.5 ±1.1 (n=47)
LGM 23-18ka
-12.9 ±1.2 (n=35)
Deglacial 18-13ka
-11.0 ±4.4 (n=96)
Density
0.00
0.25
0.50
0.75
-14
-12
-10
-8
εNd

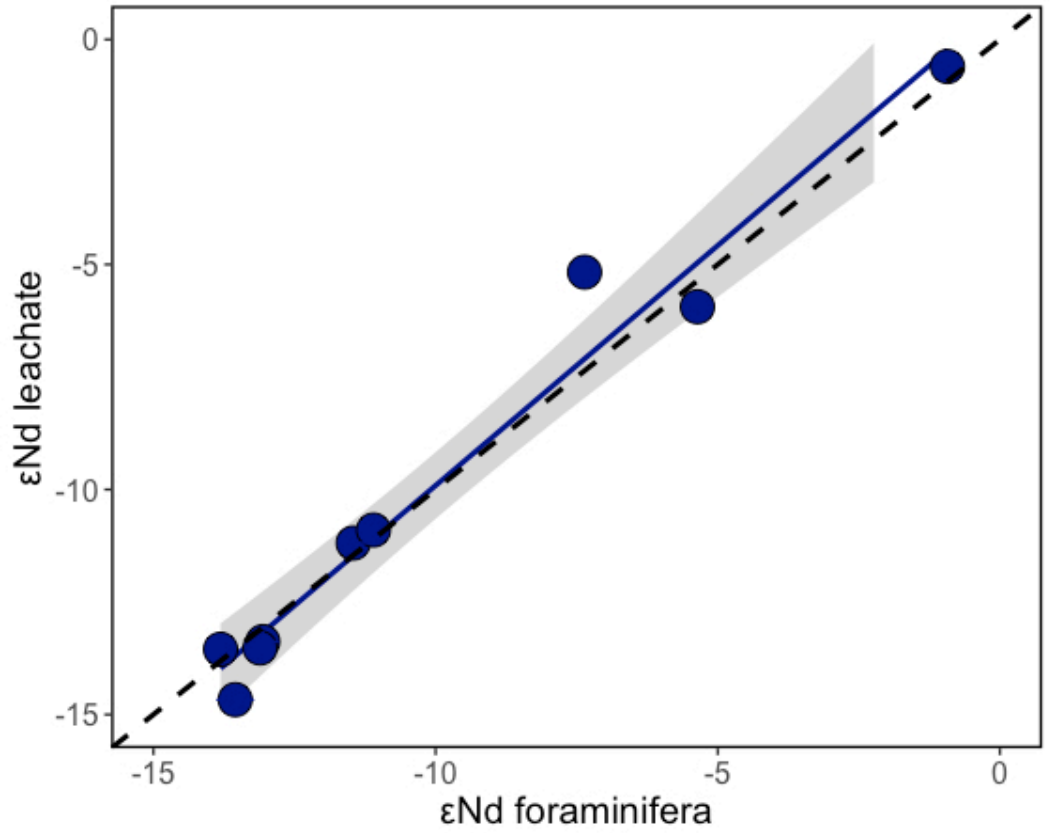
0
-5
-10
-15
εNd leachate
-15
-10
-5
0
εNd foraminifera

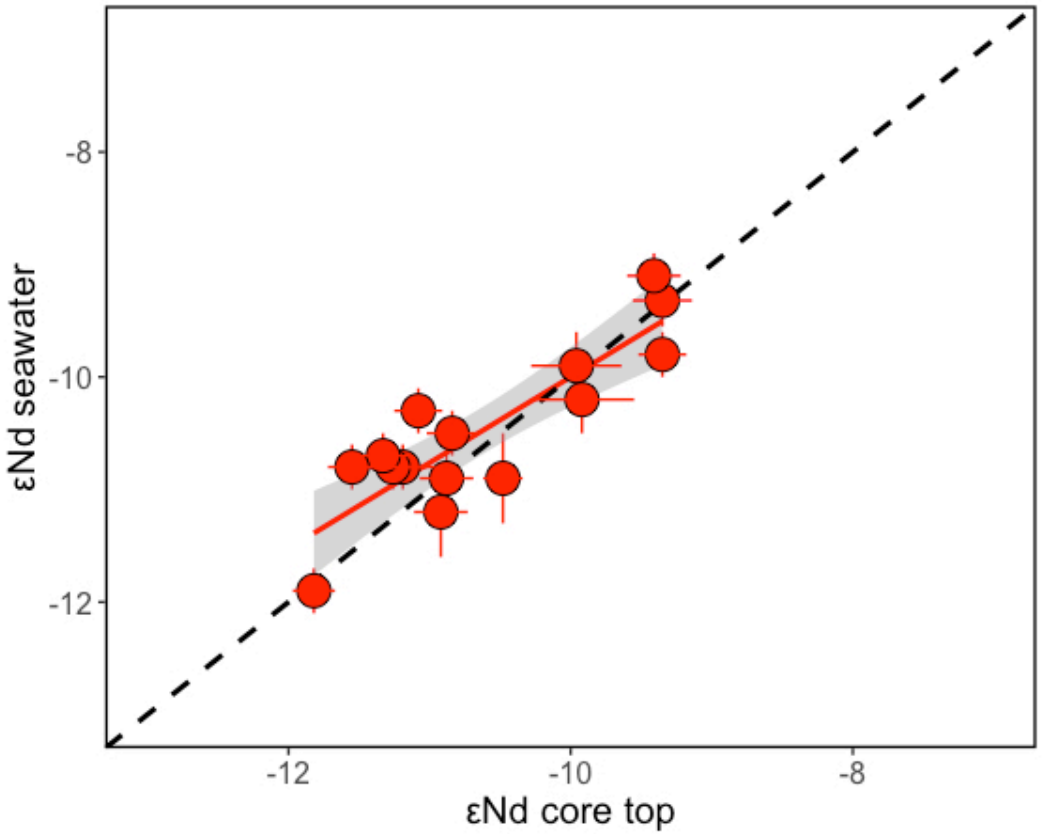
-8
-10
-12
εNd seawater
-12
-10
-8
εNd core top

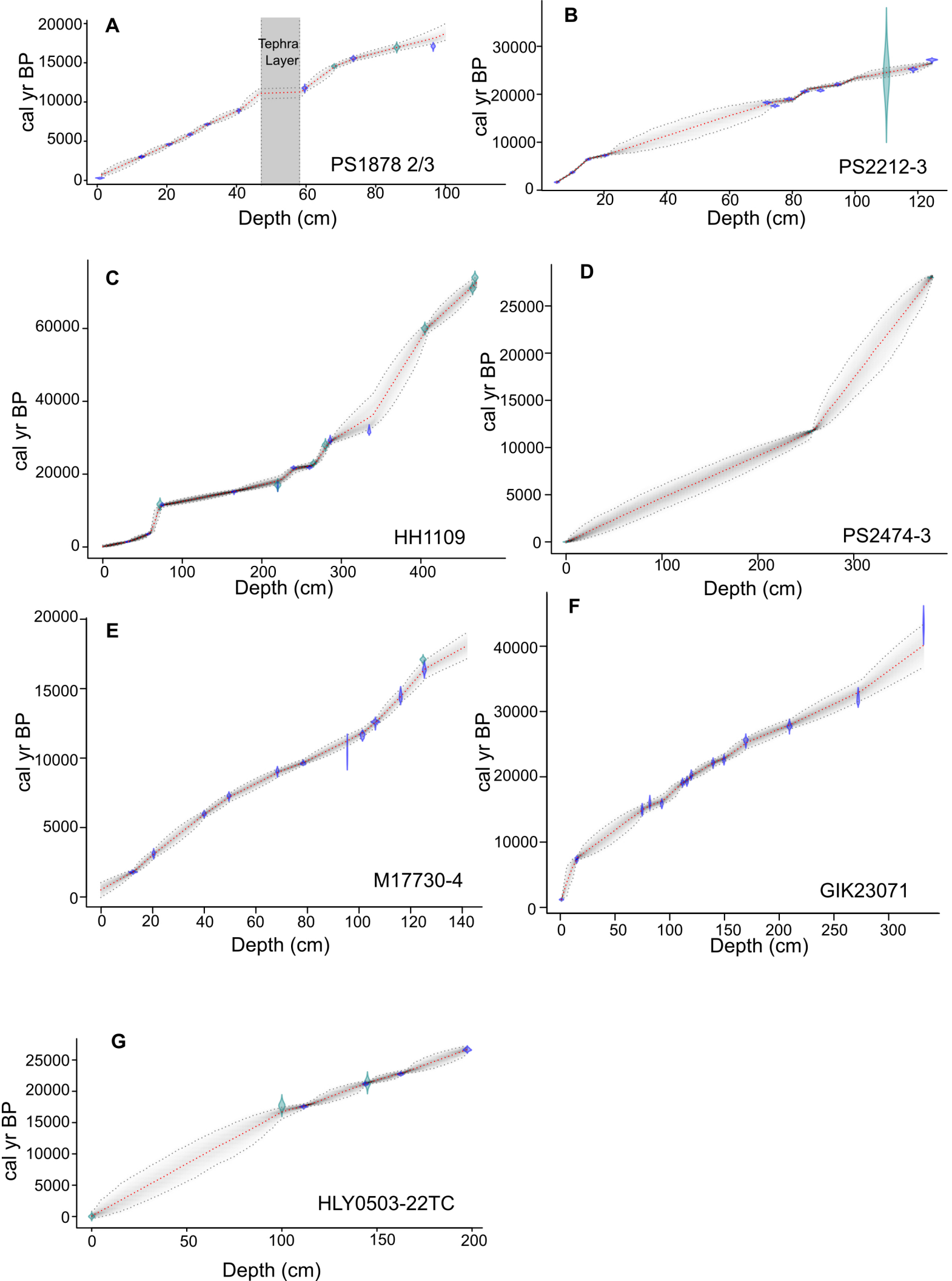
A
Tephra Layer
PS1878 2/3
cal yr BP
Depth (cm)
B
PS2212-3
C
HH1109
D
PS2474-3
E
M17730-4
F
GIK23071
G
HLY0503-22TC

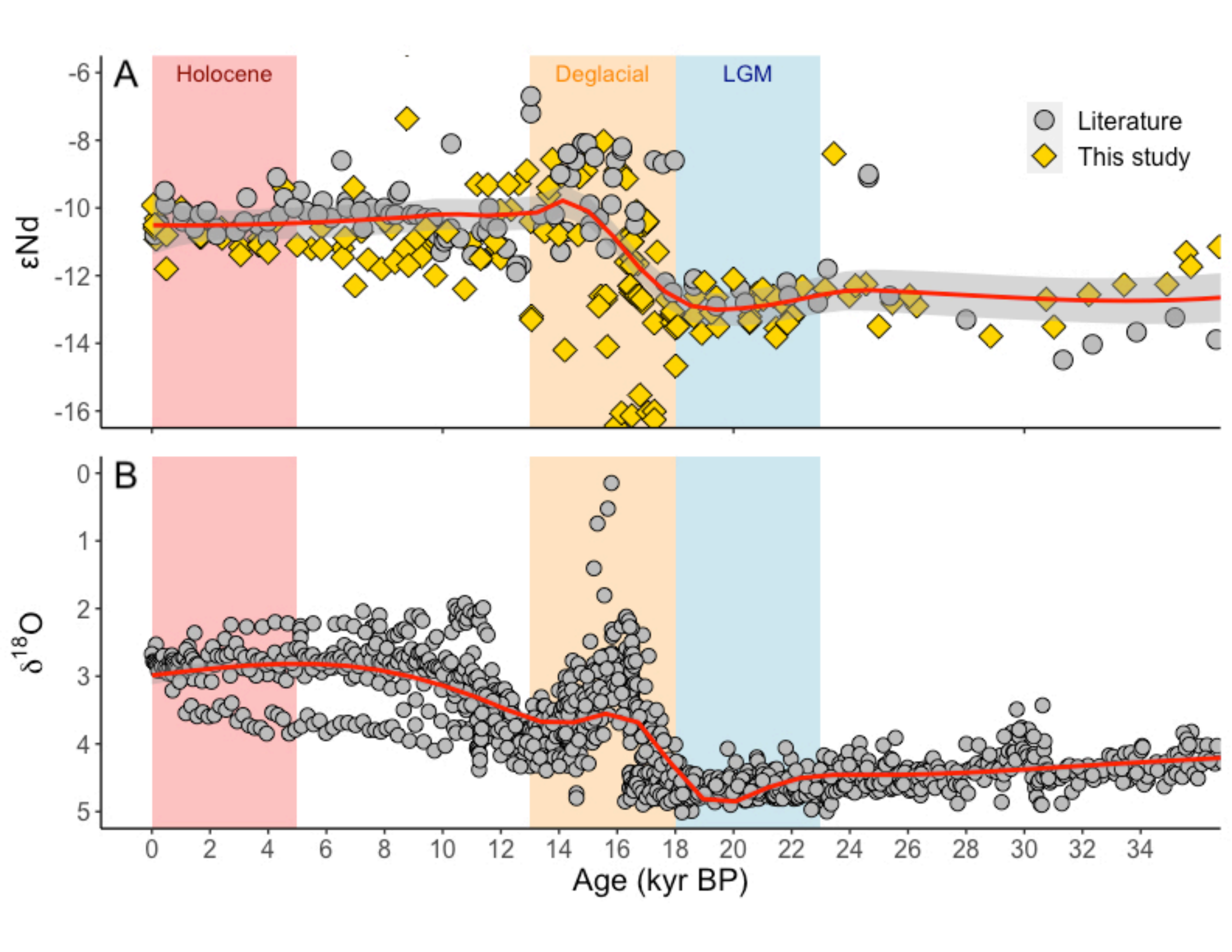
A
Holocene
Deglacial
LGM
Literature
This study
εNd
-6
-8
-10
-12
-14
-16
B
δ18O
0
1
2
3
4
5
0
2
4
6
8
10
12
14
16
18
20
22
24
26
28
30
32
34
Age (kyr BP)

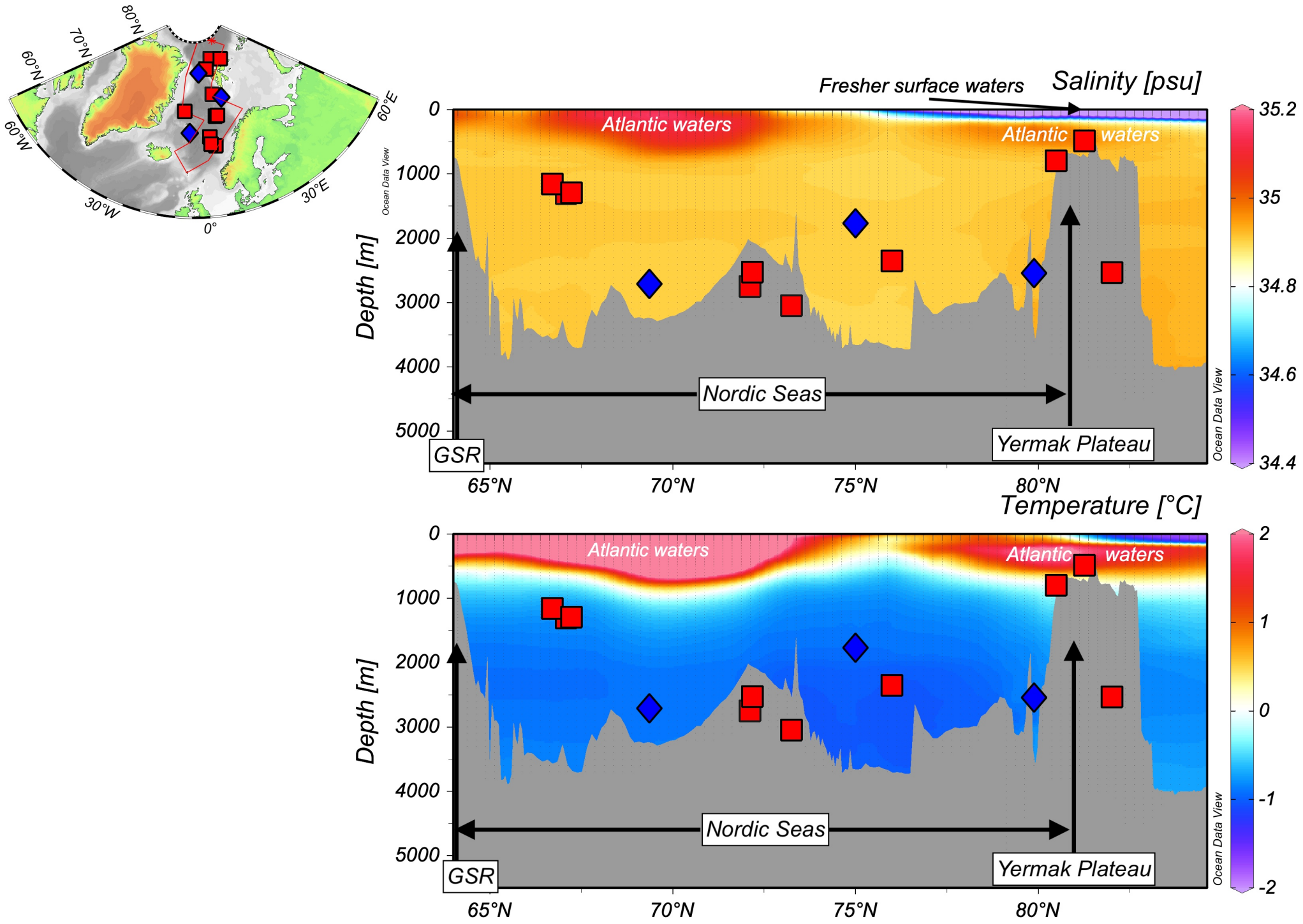
80°N
70°N
60°N
60°W
30°W
0°
30°E
60°E
Fresher surface waters
Salinity [psu]
Atlantic waters
Atlantic waters
Depth [m]
0
1000
2000
3000
4000
5000
Nordic Seas
GSR
Yermak Plateau
65°N
70°N
75°N
80°N
Ocean Data View
35.2
35
34.8
34.6
34.4
Temperature [°C]
Atlantic waters
Atlantic waters
Nordic Seas
GSR
Yermak Plateau
2
1
0
-1
-2

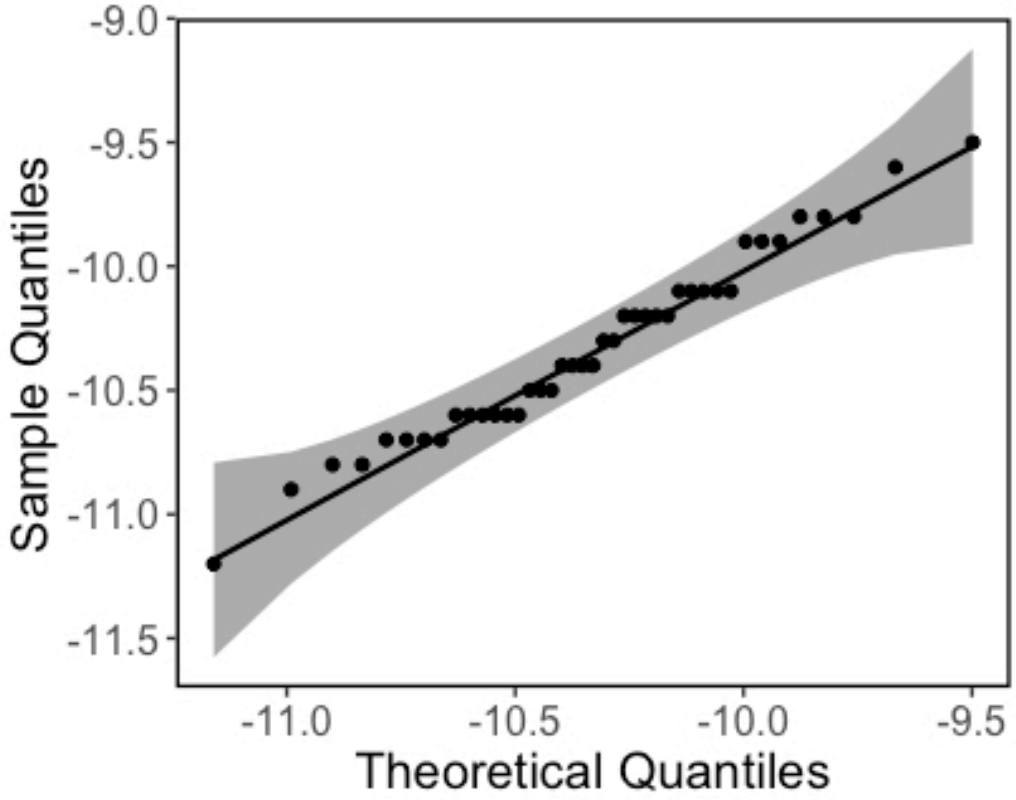
Sample Quantiles
-9.0
-9.5
-10.0
-10.5
-11.0
-11.5
-11.0
-10.5
-10.0
-9.5
Theoretical Quantiles

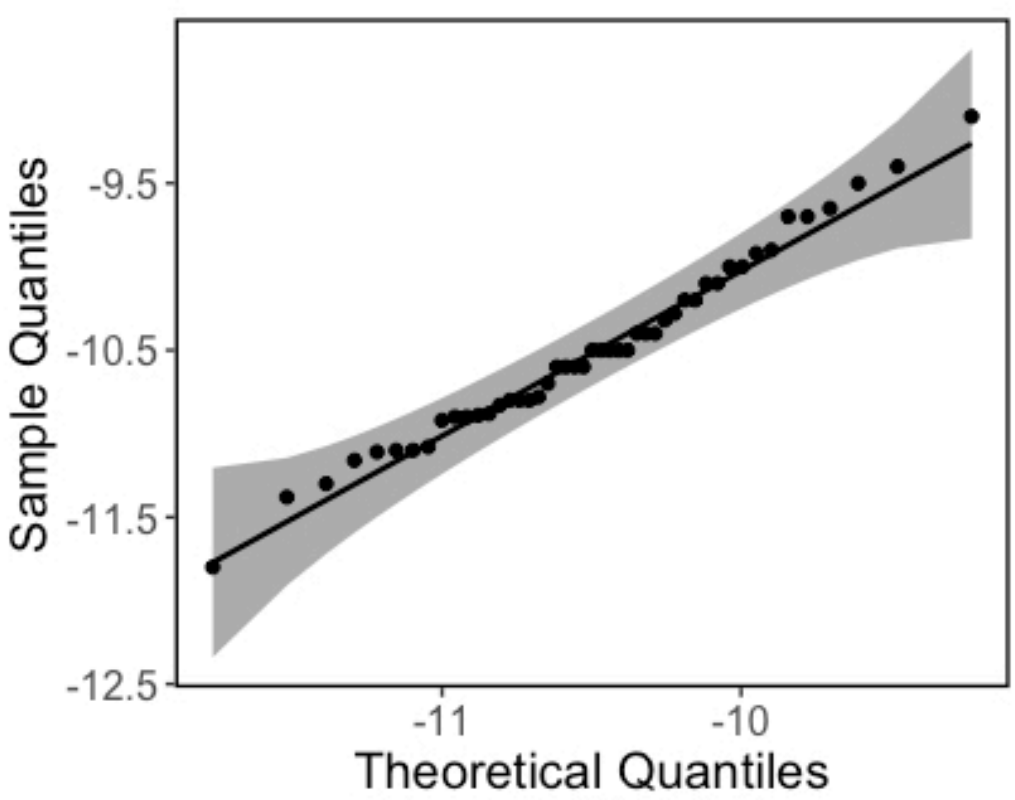
Sample Quantiles
-9.5
-10.5
-11.5
-12.5
-11
-10
Theoretical Quantiles

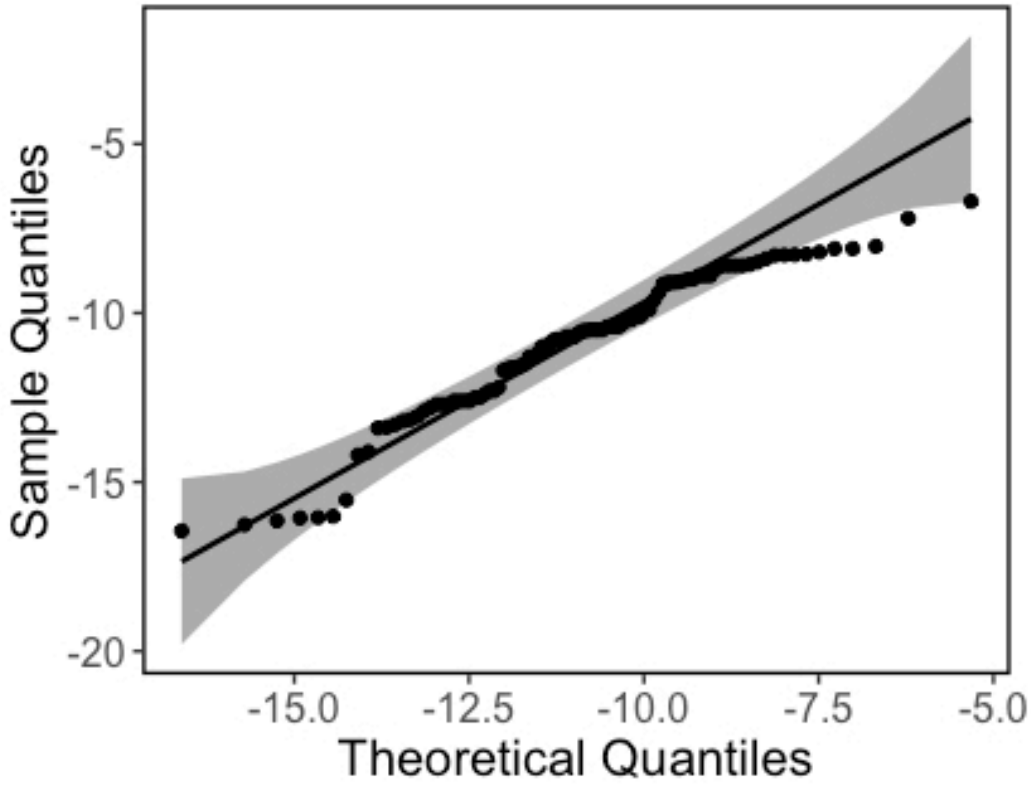
Sample Quantiles
-5
-10
-15
-20
-15.0
-12.5
-10.0
-7.5
-5.0
Theoretical Quantiles

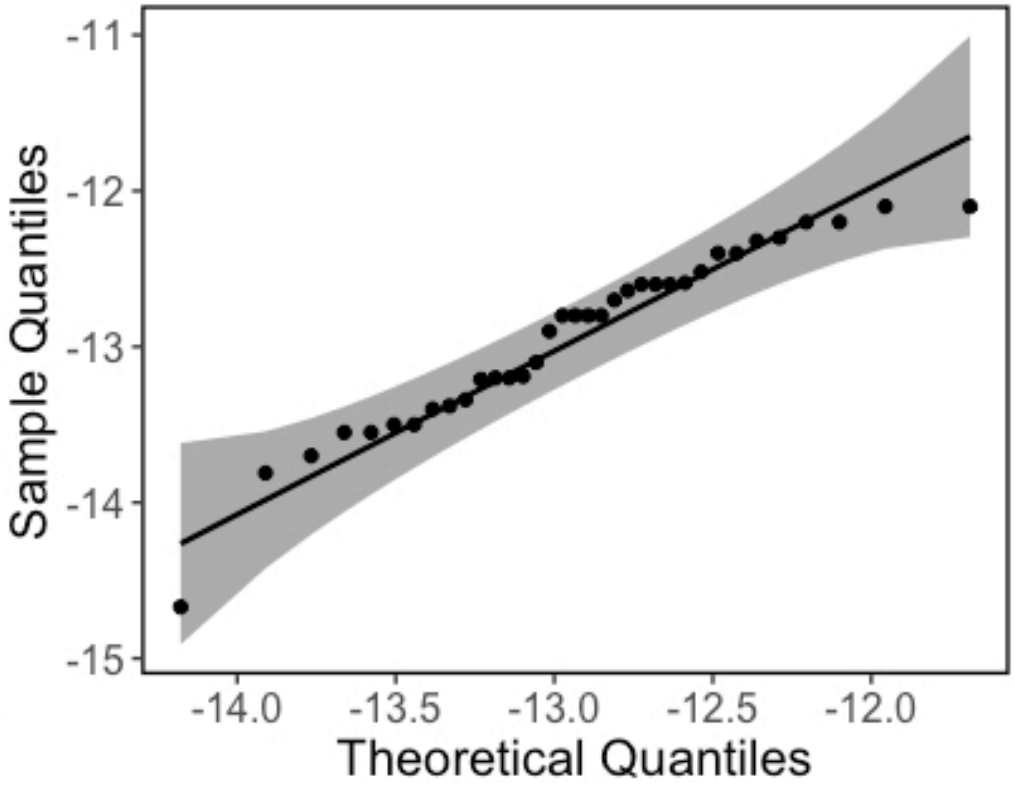
Sample Quantiles
-11
-12
-13
-14
-15
-14.0
-13.5
-13.0
-12.5
-12.0
Theoretical Quantiles

εNd Sample set	**Shapiro-Wilk test statistic, W**	***p*-value**
Modern Seawater	0.97951	0.6569
Late Holocene	0.98420	0.7579
Deglacial	0.95141	0.0010
LGM	0.94955	0.1291

εNd sample sets compared	**F-test statistic**	***p*-value**
Late Holocene and modern seawater	0.44982	0.0113
LGM and late Holocene	1.072218	0.8157